

Friction-induced shear thickening: a microscopic perspective

Moumita Maiti, Annette Zippelius, and Claus Heussinger
*Institute for Theoretical Physics, Georg-August University of Göttingen,
Friedrich-Hund Platz 1, 37077 Göttingen, Germany*
(Dated: May 12, 2018)

We develop a microscopic picture of shear thickening in dense suspensions which emphasizes the role of frictional forces, coupling rotational and translational degrees of freedom. Simulations with contact forces and viscous drag only, reveal pronounced shear thickening with a simultaneous increase in contact number and energy dissipation by frictional forces. At high densities, when the translational motion is severely constrained, we observe liquid-like gear-states with pronounced relative rotations of the particles coexisting with solid-like regions which rotate as a whole. The latter are stabilised by frustrated loops which become more numerous and persistent with increasing pressure, giving rise to an increasing lengthscale of this mosaic-like structure and a corresponding increase in viscosity.

I. INTRODUCTION

The phenomenon of shear thickening in dense suspensions of particles has caught considerable attention recently [1–11]. It is now becoming clear, through experiments and simulations, that next to the well studied hydrodynamical thickening mechanism [12–15] there is a second mechanism based on the presence or absence of inter-particle friction [3–5, 11]. Similar effects are observed in dry powders of granular particles [16–19]. Theoretically [10], it has been argued that thickening, i.e. the increase of viscosity with stress or strainrate, is due to the fact that in frictional systems the viscosity diverges at lower particle volume fractions than in the corresponding frictionless systems. For given volume fraction ϕ , the viscosity of the frictional system is therefore higher than in a frictionless reference system. Thus, by “switching-on” the frictional interactions as the stress is increased, a thickening regime occurs. Depending on how fast this switch happens, the thickening may be continuous or discontinuous. In particle-based simulations such a switch has been implemented in Ref. [7, 8, 11]. In these simulations frictional interactions are only active, when the normal force, that is pushing the particles together, exceeds a certain threshold f^* . The onset-stress for thickening then naturally follows as $\sigma_{\text{on}} = f^*/d^2$, with d the diameter of the particles.

From dimensional analysis it is clear that an additional force scale f^* is necessary, if deviations from Newtonian (or Bagnold) flow are to be seen [20]. This force scale may be implemented in various ways [4, 5, 10, 11, 16]. In Refs. [4, 16] it is introduced by giving the particles a finite stiffness. Subsequently, in these simulations, friction is not “switched-on”, but is always active, both in the thickening regime above the onset stress and in the Newtonian regime below this threshold. Thickening, then, is not a transition from frictionless to frictional rheology. It rather points to different ways frictional forces can act. Apparently, there is a qualitative change in the way frictional inter-particle forces affect the rheology at the onset of thickening. It is the goal of this article to provide a microscopic (particle-based) perspective for this change.

II. SIMULATION

We study a two-dimensional binary mixture of N soft spheres, $N/2$ spheres of diameter d and $N/2$ spheres of diameter $1.4d$. The particle volume fraction is defined as $\phi = \sum_{i=1}^N \pi R_i^2 / L^2$, where R_i is the radius of a particle i , and L is the length of the simulation box. The system is sheared along the x -direction and Lees-Edwards periodic boundary conditions are used.

Particles interact via a standard spring-dashpot interaction [21]. Two particles i, j interact when they are in contact, i.e., when their mutual distance r is smaller than the sum of their radii $R_i + R_j$. The normal component of the interaction force is $F_n = k_n[r - (R_i + R_j)] - \gamma_n \delta v_n$, where k_n is the spring constant, γ_n the dashpot strength, and δv_n the relative normal velocity of the two contacting particles. While we include this dissipative coupling γ_n in the simulations, it turns out to not play any role for the rheological behavior (see below). The tangential force component is $F_t = k_t \delta_t$, with δ_t the tangential (shear) displacement since the formation of the contact. The tangential spring mimics sticking of the two particles due to dry friction. These frictional forces are limited by the Coulomb condition $F_t \leq \mu F_n$, with a constant, i.e., velocity independent friction coefficient μ . We do not include a dissipative coefficient in the tangential direction. Still, there is tangential dissipation when contacts are sliding, via the Coulomb criterium. This choice of parameters is used primarily for simplicity in order to reduce the number of parameters. Still the essential physics is retained, namely the presence of tangential forces and dissipation.

The system is subject to shear in the x -direction. We impose a fixed shear rate $\dot{\gamma}$, which is the key control parameter of the simulation. Newtons equations of motion $m\ddot{\vec{v}}_i = \vec{F}_i^{\text{cont}} + \vec{F}_i^{\text{visc}}$ are integrated with contact forces as specified above and a viscous drag force, which implements the shear flow. The drag force $\vec{F}^{\text{visc}}(\vec{v}_i) = -\zeta \vec{\delta v}_i$ is proportional to the velocity difference $\vec{\delta v}_i = \vec{v}_i - \vec{v}_{\text{flow}}$ between the particle velocity \vec{v}_i and the flow velocity $\vec{v}_{\text{flow}}(r_i) = \hat{e}_x \dot{\gamma} y_i$ [22, 23]. The dissipative coefficient ζ

represents the viscosity of the surrounding fluid, $\zeta \sim \eta_f$. Inertial forces, while included in the equation of motion, are not important for the small strainrates considered, and only affect the flow at larger strainrates. The inertial number is generally smaller than $O(10^{-3})$.

A key difference between frictionless and frictional particles is the presence of rotational degrees of freedom. Indeed, we will argue below that the coupling of rotation and translation is an important factor in understanding the rheological properties. The equation of motion for the rotational velocity $\vec{\omega}_i$ of particle i is $I\vec{\dot{\omega}}_i = \vec{T}_i^{\text{cont}}$, where the torques derive from the contact forces given above. The torque from the viscous drag force is neglected for simplicity.

As units we use the spring constant k , the particle diameter d as well as the mass density ρ . System size is $N = 10000$ for most densities except at lower densities it is 2500. Friction coefficient and dissipative coefficients are $\mu = 1$ and $\zeta = \gamma_n = 0.1$.

III. RESULTS

The stress tensor is calculated from the virial expression, for example for the shear stress,

$$\sigma = \frac{1}{2L^2} \sum_i F_i^x y_i \quad (1)$$

where the sum is taken over all particles i . From this the viscosity is defined as $\eta = \sigma/\dot{\gamma}$. This is plotted in Fig. 1 as a function of stress σ for various volume fractions ϕ .

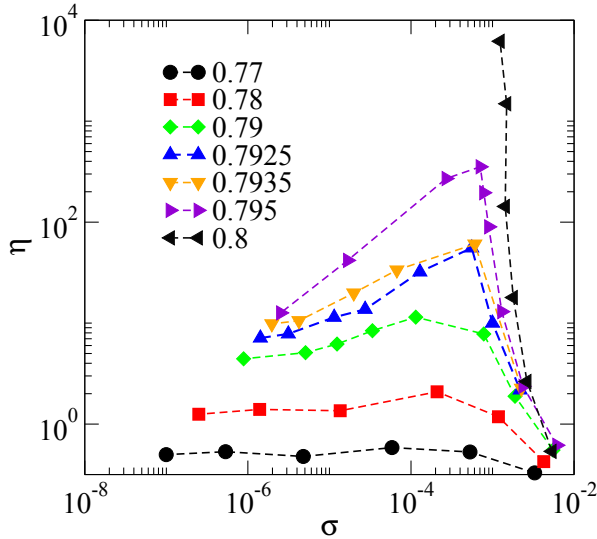


FIG. 1. Viscosity η vs. stress σ for different volume fractions ϕ .

For the smallest ϕ probed the viscosity is constant at small and intermediate stresses and then decreases. The system is shear thinning. This is also the behavior observed in a “reference” system, where frictional forces

have been switched off [22]. At slightly higher volume fractions, there is a stress value, $\sigma_{\text{on}} \approx 10^{-6}k$, above which the system displays shear thickening. The precise value for this onset stress is difficult to obtain, as the associated strainrates are very small and simulations get prohibitively long. Such a thickening regime is absent in the frictionless reference system. At still higher ϕ the viscosity is infinite below the yield stress $\sigma_y \approx 10^{-3}k$ and the system is solid there. The small prefactor for the onset of thickening already indicates that this phenomenon is not straightforwardly related to the direct particle interactions but is rather a many-body network effect.

From the diagonal elements of the stress tensor, i.e. the pressure p , we obtain a similar behavior. The (macroscopic) friction coefficient $\mu_m = \sigma/p$ only slightly varies between 0.29 and 0.31.

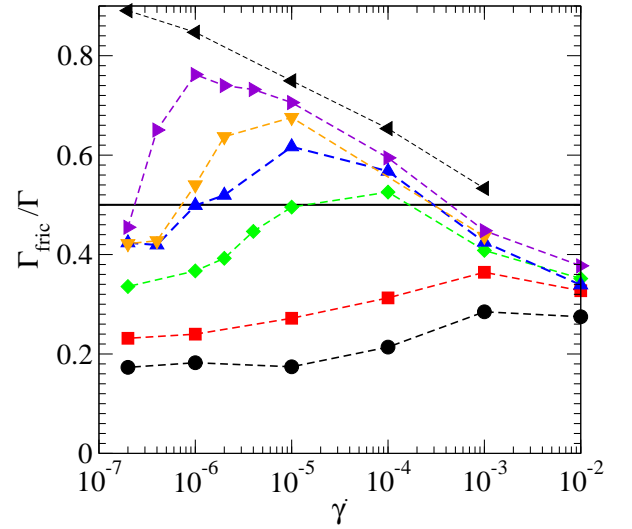


FIG. 2. Fraction of energy dissipated via frictional interactions $\Gamma_{\text{fric}}/\Gamma$ vs. strainrate $\dot{\gamma}$ for different volume fractions ϕ . Color code as in Fig. 1.

While the crucial role of friction for the shear thickening behavior is demonstrated from the comparison with the frictionless reference system, we can quantify this influence by calculating the amount of energy dissipation that is due to frictional forces. The viscosity η is quite generally connected to the total energy dissipation rate $\Gamma = L^2\eta\dot{\gamma}^2$. To determine the contribution Γ_{fric} from frictional forces we calculate the viscous contribution as [24]

$$\Gamma_{\text{visc}} = \zeta N \langle \delta v^2 \rangle \quad (2)$$

where δv is the non-affine particle velocity $v - v_{\text{flow}}$, i.e. after the flow velocity is subtracted. The frictional contribution then is $\Gamma_{\text{fric}} = \Gamma - \Gamma_{\text{visc}}$ (the dissipation from inelastic collisions is very small and can be neglected). The ratio $\Gamma_{\text{fric}}/\Gamma$ is plotted in Fig. 2 for the same data as in Fig. 1. Most notably is the strong increase of the frictional contribution in the thickening regime. However, friction also plays a non-negligible role when no thickening is observed (at lower ϕ and small strainrates).

In previous work [4] we have argued that the viscous dissipation induced by particle translational velocities is coupled to a length-scale that occurs in the spatial correlation of velocities $C_v = \langle \delta v(x) \delta v(0) \rangle$. The long-range part of the correlation function decays exponentially, $C_v \sim e^{-x/\xi_v}$, giving rise to a length-scale $\xi_v(\dot{\gamma})$ that was shown to increase in the thickening regime [4, 25]. Examples of this correlation function are displayed in Fig. 4 of Ref. [4]. Here we furthermore show that this correlation length ξ_v is tightly connected to the fluctuations of the particle velocity $\delta v \equiv \sqrt{\langle \delta v_i^2 \rangle}$. Fig. 3 emphasizes that both quantities are proportional to each other, with a proportionality constant of order unity, $\delta v \approx 1.7 \xi_v \dot{\gamma}$. This indicates that typical velocities are no longer set by the size of the particles as $v \sim d \dot{\gamma}$, rather the fundamental length-scale is now the correlation length ξ_v , which takes the meaning of an effective particle size. It needs to be emphasized that this proportionality is a nontrivial result, as it represents a direct link between a single-particle observable (the velocity) and a two-point correlation function. As, according to Eq. (2), the velocities enter the viscous dissipation rate $\Gamma_{\text{visc}} \sim \delta v^2$, we need to have $\Gamma_{\text{visc}} \sim \xi_v^2 \dot{\gamma}^2$, for consistency. This is indeed observed in Fig. 4 (open symbols). Interestingly, the frictional contribution to the energy dissipation rate Γ_{fric} scales differently, $\Gamma_{\text{fric}} \sim \xi_v^3 \dot{\gamma}^2$ (filled symbols in Fig. 4). The additional factor of ξ_v as compared to Γ_{visc} can be understood by noting that the frictional dissipation can be written as $\Gamma_{\text{fr}} \sim (\mu f_n) \cdot \delta v$, which is just the dissipation of a sliding contact, sliding at velocity $\delta v \sim \xi_v \dot{\gamma}$ under normal force f_n . Assuming that predominantly viscous forces lead to the build-up of the normal force, we can write $f_n \sim \Gamma_{\text{visc}}/\dot{\gamma} \sim \xi_v^2 \dot{\gamma}$ and, consequently, $\Gamma_{\text{fric}} \sim \xi_v^3 \dot{\gamma}^2$.

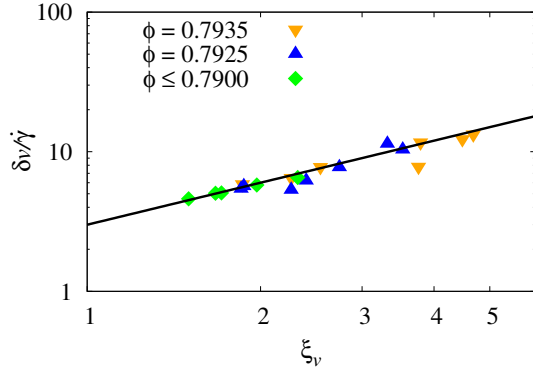


FIG. 3. Normalized translational velocity $\delta v/\dot{\gamma}$ vs. correlation lengthscale ξ_v . Velocity is proportional to length scale, $\delta v \approx 1.7 \xi_v \dot{\gamma}$.

In order to better understand the microscopic origins of these phenomena we first take a look at the average number of contacts per particle, z (see Fig. 5). In the zero-stress limit the connectivity is below the isostatic value of $z_{\text{iso}} = 3$, as expected for a fluid. The isostatic

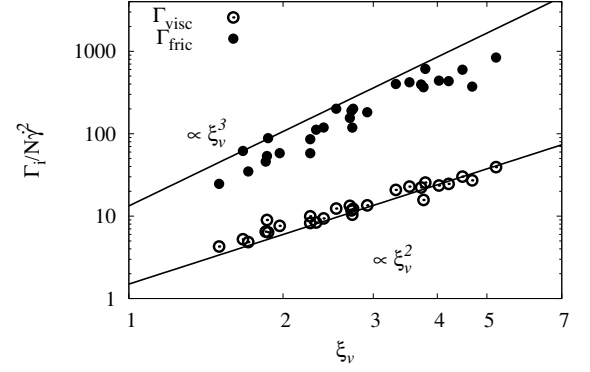


FIG. 4. Normalized energy dissipation $\Gamma_i/N\dot{\gamma}^2$ vs. length-scale ξ_v , where i stands for viscous (visc) and frictional (fric) contributions, respectively. The frictional contribution is multiplied by ten to avoid overlapping data points. Data taken from different strainrates, volume fractions and system sizes.

point represents the minimal connectivity value at which a jammed state can first be formed. Typically, however, and depending on the preparation procedure, frictionally jammed states have a somewhat higher coordination, $z_{\text{jam}} > z_{\text{iso}}$ [26, 27]. With increasing stress, in the thick-

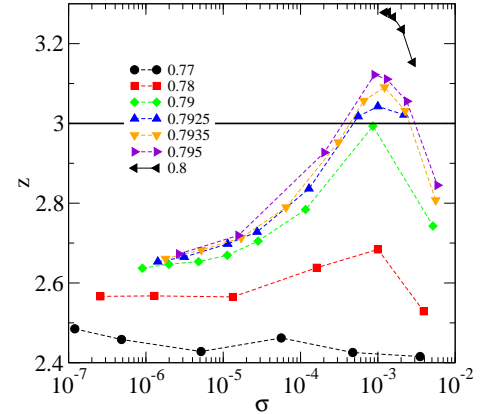


FIG. 5. Average number of contacts per particle z vs. stress for different volume fractions. At the onset of thickening the connectivity starts to rise and peaks at the yield-stress with $z \approx z_{\text{iso}}$.

ening regime, also z increases. At the yield-stress σ_y our system is approximately isostatic, before the connectivity decreases again in the regime of shear-thinning. The latter effect is also observed in the frictionless reference system, however, the increase of z with stress (or pressure) is special for the frictional system.

In the thickening regime, we also observe a universal functional dependence $z(\sigma)$, as the connectivity only weakly depends on volume fraction ϕ . One may therefore identify the connectivity as the relevant field that triggers the onset of thickening.

More detailed information about the inter-particle con-

tacts is given by the probability distribution for z . To this end we use a slightly coarse-grained version q of the connectivity. To calculate q , the particle based contact number z is averaged over a circular region of radius $R = 3$. This value for the coarse-graining parameter corresponds roughly to the second minimum in the pair correlation function. In Fig. 6 the probability distribution $P(q)$ is shown for different strainrates and $\phi = 0.7935$. Most notably, a distinctive shoulder at $q \approx z_{\text{iso}} = 3$ develops in the thickening regime. Thus, thickening is associated with the formation of local patches of elevated connectivity.

This is in close analogy to the recent work of Henkes *et al.* [28], that observe a distribution of rigid clusters, the typical size of which diverges when crossing the jamming transition. It is tempting to identify these clusters with our regions of elevated connectivity, as well as their size with the above introduced length-scale ξ_v .

Shear thickening then corresponds to the formation of temporarily rigid clusters in a sea of floppy particles. The role of pressure is to stabilize these clusters as frictional contacts get more stable for higher pressures. As pressure increases with increasing strainrate, the size of these regions grows larger, and dissipation is increased via the contributions presented in Fig. 4. All this is not observed in frictionless systems. Indeed, Ref. [28] claims that no diverging cluster size is observed without friction.

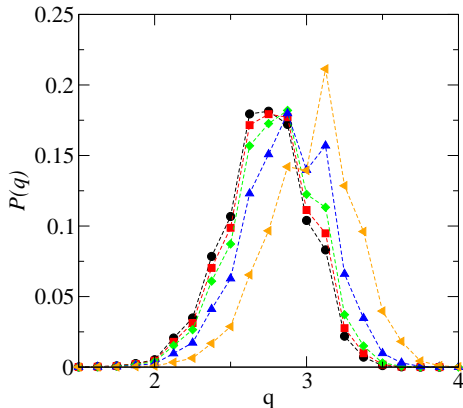


FIG. 6. Probability distribution $P(q)$ of the coarse-grained contact number q , for the volume fraction $\phi = 0.7935$ and different strainrates $\dot{\gamma} = 2 \times 10^{-7}$ (black circles), 4×10^{-7} (red squares), 10^{-6} (green diamonds), 2×10^{-6} (blue triangles up), 4×10^{-6} (orange triangles left).

A key difference between frictional and frictionless particles is the presence of rotational degrees of freedom. Fig. 7 indicates that particle rotations are strongly coupled to translations. The root-mean square fluctuations of the rotational velocity $\delta\omega$ is always about three times the translational velocity δv . With this one may anticipate that rotational correlations are also coupled to translational correlations, i.e. characterized by a similar lengthscale as ξ_v introduced above. To test this assumption we define $C_{|\omega|}(x) = \langle \delta|\omega(x)|\delta|\omega(0)| \rangle$ for the correla-

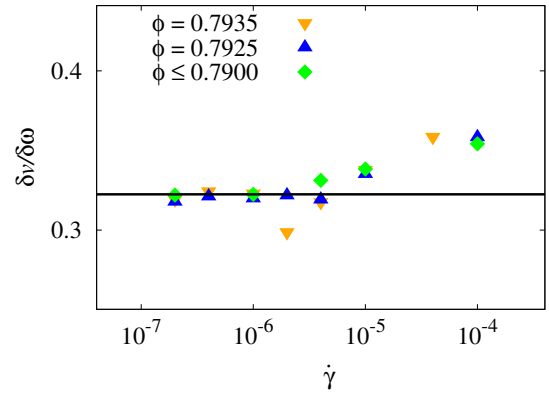


FIG. 7. Ratio of translational to rotational velocity vs. strainrate $\dot{\gamma}$. The ratio is nearly constant, $\delta v / \delta \omega \approx 0.32d$; note the linear y-axis.

tion of the absolute values of particle rotations. Fig. 8 indicates that this function acquires a long-range decay in the shear-thickening regime. While the decay is not strictly exponential, we have tried to fit a function of the form $\sim \exp(-x/\xi_\omega)$, where $\xi_\omega = c\xi$ with a universal constant $c \approx 2.3$. This procedure works very well so that we can conclude that the correlations of translational and rotational velocities are indeed governed by the same lengthscale $\xi \propto \xi_v \propto \xi_\omega$.

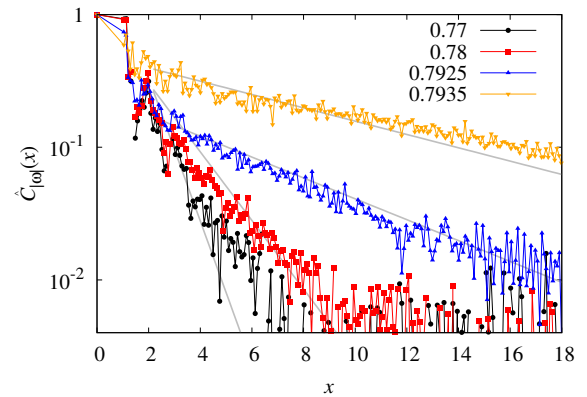


FIG. 8. Normalized correlation function $\hat{C}_{|\omega|}(x) = C_{|\omega|}(x) / \langle \delta|\omega|^2 \rangle$ vs. x for $\dot{\gamma} = 10^{-6}$ and different $\phi = 0.77, 0.78, 0.7925, 0.7935$. The grey lines are fits using an exponential function $\sim \exp(-x/\xi_\omega)$, where $\xi_\omega = 2.3\xi_v$.

To understand the reason and the consequences of the coupling between rotations and translations consider the situation that two individually rotating particles come into contact. Once the contact is formed, the frictional forces will act to reduce the relative tangential motion of the two particles at the point of contact, up until the condition $v_1 - v_2 = (d_1\omega_1 + d_2\omega_2)/2$ is met, when there is no relative motion at the point of contact.

One may think of two extreme scenarios to achieve this goal: either rotations adapt (via frictional dissipa-

tion) without generating relative translational motion, $v_1 \approx v_2$. In this case particles will rotate at the same speed in opposite sense, i.e. $\omega_1 = -\omega_2$ (equal-sized particles). Alternatively, rotational velocity may be transformed in translational velocity, $v \sim d\omega$. In this case particles will rotate around each other instead of around their respective particle centers. Such a motion leads to viscous dissipation.

In general contacts do not come in pairs, and particles are tightly constrained by the surrounding network of other contacts. We have quantified this influence via the lengthscale ξ that governs the correlations of particle velocity. In extension to the two-particle picture of contact formation we can therefore think of a patch of particles of linear size ξ . In this patch, particles are either (in the extreme cases just discussed) rotating coherently without relative slip and with only little movement in space, or they are translating more or less as solid blocks forming clusters or vortices [22, 29, 30]. Such a behavior can be seen in Fig. 9. The state of rotation of particles is displayed together with their nonaffine velocities. Most prominent are the vortex- or block-like structures in places where the rotational velocities are small (particles are only shown when their rotational velocity is large.)

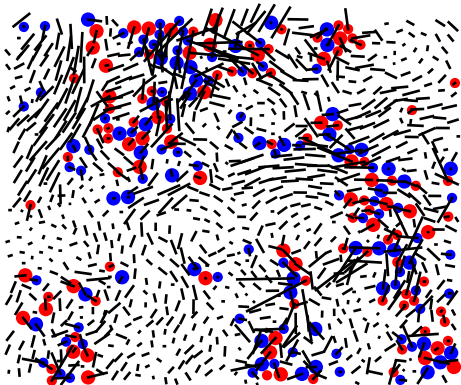


FIG. 9. Snapshot of a small part of the system at $\dot{\gamma} = 10^{-6}$ and $\phi = 0.7925$. Color code represents the rotational state of the particles (only strongly rotating particles are shown): large clockwise rotation (red), large anti-clockwise (blue). Lines are the non-affine velocities of the particles. Clusters and vortices seem to form in between clusters of strongly rotating particles.

The state of coherent rotations without slip has been called a bearing-state [31, 32]. Because of the counter-rotation of neighboring particles the typical particle rotation $\delta\omega \sim \dot{\gamma}(\xi/d)$ in such a state is much larger than the average rotation, which can be taken to be imposed by the strainrate of deformation, $\bar{\omega} \sim \dot{\gamma}$ [33]. Such a counter-rotation is readily observed in the exemplary snapshot of Fig. 10, where connected particles typically show alternating sign of their rotational velocity. A similar conclusion is obtained from the correlation function of particle rotations, $C_\omega(r) = \langle \delta\omega(0)\delta\omega(r) \rangle$ (without absolute values) as displayed in Fig. 11. Contacting particles (those

at distances, $r = 1.0, 1.2, 1.4$) have a strongly negative correlation of their rotational velocities.

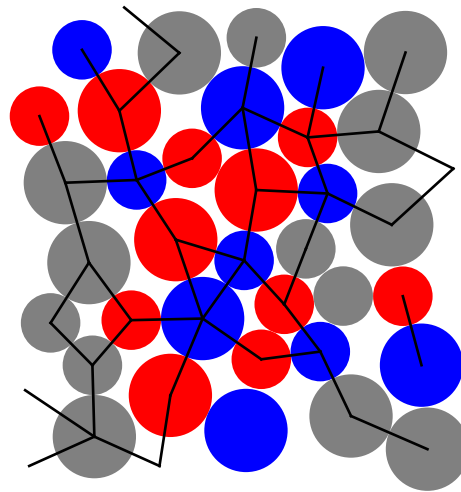


FIG. 10. Snapshot of a small part of the system at $\dot{\gamma} = 10^{-6}$ and $\phi = 0.7925$. Color code represents the rotational state of the particles: small rotation (gray), large clockwise (red), large anti-clockwise (blue). Contacts are indicated by lines between particles. Note the alternating color of connected particles highlighting the strong rolling motion.

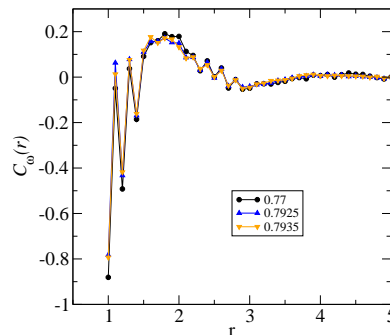


FIG. 11. Normalized correlation function $\hat{C}_\omega(r) = \langle \delta\omega(0)\delta\omega(r) \rangle / \langle \delta\omega^2 \rangle$ (no absolute values as compared to Fig. 8) vs. distance r . Strong anti-correlation of contacting particles (those at $r = 1.0, 1.2, 1.4$).

However, not all contact networks allow for bearing states. A crucial role is played by contact loops. A contact loop is a set of contacting particles that form an “empty” loop, i.e. with no other (contacting) particle inside the loop. A k -loop then is a contact loop with k particles. Loops with an odd number of particles, in particular three-particle loops, play an important role in the process of rotational frustration [34]. These loops do not allow for coherently rotating states and rotation is fully frustrated, similar to the spins in antiferromagnetic triangular plaquettes.

It has been argued that the presence of these loops stabilize the contact network in packings of granular particles, for example, by inhibiting the buckling of force

chains [31, 35]. In a dynamic setting during shear flow there is a constant breaking-up of smaller loops into larger ones, and the reverse process of collapse of larger loops into smaller ones. The presence of 3-loops then inhibits gear states and favors the formation of blocks or vortices. This increases energy dissipation and leads to the shear-thickening state.

From the Euler characteristic the total number of loops per particle only weakly increases with the connectivity as $n_l = (z/2 - 1)$. By way of contrast, as is evidenced by Fig. 12 the number of 3-loops strongly increase when entering the thickening regime – roughly by a factor of three.

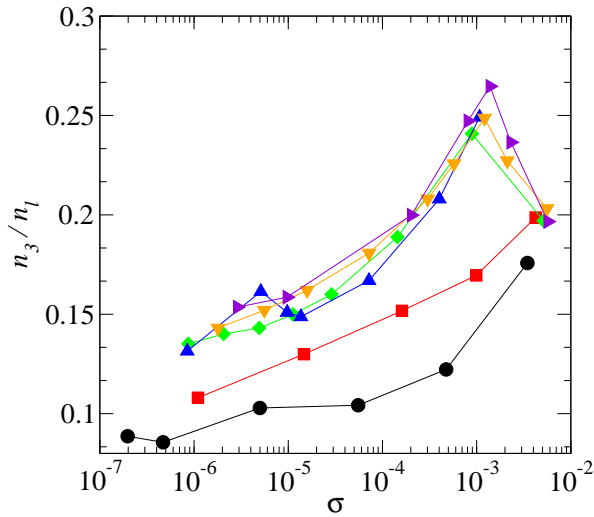


FIG. 12. Fraction n_3/n_l of 3-particle loops vs. stress σ for different ϕ . Color coding is as in Fig. 1.

One can therefore think of a 3-loop as a defect with the lengthscale ξ playing the role of the defect size. Once contact rotation becomes frustrated the rotational velocity of the individual particles can be turned into translational velocity of a structure of size ξ , the velocity scaling as $\delta v \sim \dot{\gamma}\xi$. The viscous dissipation then follows as $\Gamma_v \sim \zeta \delta v^2 \sim \xi^2$.

IV. CONCLUSION

We study the phenomenon of shear thickening in dense athermal suspensions. The mechanism responsible for shear thickening is agreed to consist of a transition from frictionless to frictional rheology. However, it is not clear how this transition comes about on the microscopic level of particles. In this work we have started to fill this gap of understanding. The goal is to provide particle-based explanations of how structural, dynamical and rheological properties change in the shear-thickening regime at high particle volume fractions. In line with recent work we have observed that shear thickening is associated with

increased frictional interactions. We have quantified this importance by measuring the amount of energy that is dissipated via frictional forces. Nevertheless, frictional dissipation is also present in the Newtonian regime and can never be neglected. This points to different ways frictional forces may act. A clue to this variability is provided by the presence of the correlation lengthscale ξ , that shows up in the spatial correlations of particle translational and rotational velocities, and which starts to grow at the onset of thickening. Subsequently, the lengthscale governs viscous and frictional energy dissipation as $\Gamma_{\text{visc}} \sim \xi^2 \dot{\gamma}^2$ and $\Gamma_{\text{fric}} \sim \xi^3 \dot{\gamma}^2$, respectively. On the kinematic side, the length-scale sets the scale for the particle velocities, the fluctuating (non-affine) contributions scaling as $\delta v \sim \xi \dot{\gamma}$. The key difference between frictionless and frictional systems is the presence of rotational degrees of freedom. We have found that rotational velocities are strongly coupled to translations, their ratio being nearly constant ($\delta v / \delta \omega \approx 0.32$) throughout the thickening regime. Thus, also rotational velocities scale with the correlation lengthscale, $\delta \omega \sim (\xi/d) \dot{\gamma}$.

We have interpreted these findings with the help of the concept of rotational frustration, that occurs whenever new contacts lead to loops with an odd number of particles. These loops block the coherent rotation of a particle patch and favor the interchange of rotational into translational velocities. In consequence, the particles start to move as (temporarily) rigid clusters and viscous energy dissipation is enhanced.

Pressure is expected to play an important role in these processes. At small pressures these structures quickly relax, and the resulting shear stability is weak. At higher pressures, in the thickening regime, these structures persist resulting in a higher stability. In this picture the system consists of a mosaïque of solid-like blocks or vortices (maybe formed by frustrated loops) and liquid-like gear-states (see Fig. 10). Vortex particles do not rotate, but vortices rotate as solid bodies. Gear particles, in contrast, strongly rotate relative to each other. The size of these structures increases as pressure increases, and so does the viscosity. There are striking similarities with the recent work of Henkes *et al.*[28]. By implementing a rigid cluster decomposition they detect temporarily rigid particle patches, the typical size of which diverges when crossing the jamming transition. In that work the approach to jamming is associated with increasing volume fraction, while here we deal with (presumably) the same phenomenon as a function of strainrate to explain the shear-thickening state. More work will be necessary to fully work out these analogies.

ACKNOWLEDGMENTS

We acknowledge financial support by the German Science Foundation via the Emmy Noether program (He 6322/1-1).

-
- [1] E. Brown and H. M. Jäger, Rep. Prog. Phys. **77**, 046602 (2014).
 - [2] A. Fall, N. Huang, F. Bertrand, G. Ovarlez, D. Bonn, Phys. Rev. Lett. **100**, 018301 (2008).
 - [3] E. Brown, and H. M. Jaeger, J. Rheol. **56**, 875 (2012).
 - [4] C. Heussinger, Phys Rev. E **88**, 050201(R) (2013).
 - [5] N. Fernandez, R. Mani, D. Rinaldi, D. Kadau, M. Mosquet, H. Lombois-Burger, J. Cayer-Barrioz, H. J. Herrmann, N. D. Spencer, and L. Isa, Phys. Rev. Lett. **111**, 108301 (2013).
 - [6] Z. Pan, H. de Cagny, B. Weber, and D. Bonn, Phys. Rev. E **92**, 032202 (2015).
 - [7] R. Mari, R. Seto, J. F. Morris and M. Denn, Phys. Rev. E **91**, 052302 (2015).
 - [8] R. Mari, R. Seto, J. F. Morris, and M. M. Denn, J. Rheol. **58**, 1693 (2014).
 - [9] A. Fall, F. Bertrand, D. Hautemayou, C. Meziere, P. Moucheron, A. Lemaitre, and G. Ovarlez, Phys. Rev. Lett. **114**, 098301 (2015).
 - [10] M. Wyart, and M. E. Cates, Phys. Rev. Lett. **112**, 098302 (2014).
 - [11] R. Seto, R. Mari, J. F. Morris and M. M. Denn, Phys. Rev. Lett. **111**, 218301 (2013).
 - [12] X. Bian, S. Litvinov, M. Ellero, and N. J. Wagner, J. Non-Newt. Fluid Mech. **213**, 39 (2014).
 - [13] N. J. Wagner, and J. F. Brady, Phys. Today **62**, 27 (2009).
 - [14] J. F. Brady, and G. Bossis, J. Fluid Mech. **155**, 105 (1985).
 - [15] X. Cheng, J. H. McCoy, J. N. Israelachvili, and I. Cohen, Science **333**, 1276 (2011).
 - [16] M. Grob, C. Heussinger and A. Zippelius, Phys. Rev. E **89**, 050201(R) (2014).
 - [17] M. Otsuki, and H. Hayakawa, Phys. Rev. E **80**, 011308 (2009).
 - [18] D. Bi, J. Zhang, B. Chakraborty, and R. Behringer, Nature (London) **480**, 355 (2011).
 - [19] S. Sarkar, and B. Chakraborty, Phys. Rev. E **91**, 042201 (2015).
 - [20] G. Lois, A. Lemaître, and J. M. Carlson, Phys. Rev. E **76**, 021302 (2007).
 - [21] P. A. Cundall, and O. D. L Strack, Geotechnique, **29**, 47 (1979).
 - [22] P. Olsson and S. Teitel, Phys. Rev. Lett. **99**, 178001 (2007).
 - [23] D. J. Durian, Phys. Rev. Lett. **75**, 4780 (1995).
 - [24] B. Andreotti, J.-L. Barrat, and C. Heussinger, Phys. Rev. Lett. **109**, 105901 (2012).
 - [25] We find a similar lengthscale in the granular powder simulations of Ref. [16]; unpublished.
 - [26] I. Agnolin and J.-N. Roux, Phys. Rev. E **76**, 061302 (2007).
 - [27] C. Song, P. Wang, and H. A. Makse, Nature **453**, 629 (2008).
 - [28] S. Henkes, D. A. Quint, Y. Fily, and J. M. Schwarz, Phys. Rev. Lett. **116**, 028301 (2016).
 - [29] Heussinger, C., Berthier, L., and Barrat, J.-L., EPL **90**, 20005 (2010).
 - [30] A. Tanguy, J. P. Wittmer, F. Leonforte, and J.-L. Barrat, Phys. Rev. B **66**, 174205 (2002).
 - [31] J. A. Aström, H. J. Herrmann, and J. Timonen, Phys. Rev. Lett. **84**, 638 (2000).
 - [32] F. Alonso-Marroquin, I. Vardoulakis, H. J. Herrmann, D. Weatherley, and P. Mora, Phys. Rev. E **74**, 031306 (2006).
 - [33] T. C. Halsey, Phys. Rev. E **80**, 011303 (2009).
 - [34] A. Tordesillas, D. M. Walker, G. Froyland, J. Zhang, and R. P. Behringer, Phys. Rev. E **86**, 011306 (2012).
 - [35] A. Tordesillas, D. M. Walker, and Q. Lin, Phys. Rev. E **81**, 011302 (2010).